IEEE Access
Multidisciplinary | Rapid Review | Open Access Journal

SPECIAL SECTION ON RECONFIGURABLE INTELLIGENT SURFACE AIDED COMMUNICATIONS FOR 6G AND BEYOND

Received August 31, 2021, accepted September 16, 2021, date of publication September 20, 2021, date of current version October 13, 2021.

Digital Object Identifier 10.1109/ACCESS.2021.3113917

Capacity Improvement in Reconfigurable Intelligent Surface Assisted MIMO Communications

JUN YANG, YIJIAN CHEN, MENGNAN JIAN, JIANWU DOU, AND MIN FANG

State Key Laboratory of Mobile Network and Mobile Multimedia Technology, Shenzhen 518055, China
Wireless Product Research and Development Institute, ZTE Corporation, Shenzhen 518057, China

Corresponding author: Jun Yang (yang.jun10@zte.com.cn)

This work was supported by ZTE Corporation.

ABSTRACT Reconfigurable intelligent surface (RIS) is thought to be a potential key technique for future wireless communications due to its ability for manipulating the electromagnetic environment smartly. This paper focuses on the rank and capacity analysis when a RIS is introduced into a multiple-input multiple-output (MIMO) system. By establishing a system model for this communication system, various simulations are conducted for identifying the characteristics of the channel. The simulations of different distance between the access point (AP) and user equipment (UE) show that the condition number of the channel is worsen when the distance increases and the role of the RIS in rank improvement is weaken. The spatial distributions of the reciprocal condition number of the channel which corresponds to the RIS locations are obtained and rank-deficient zones are found in different AP, UE and RIS configurations, which depicts the spatial characteristics of the RIS-assisted MIMO channel. The simulations also indicate that the condition number of the channel not only varies with the RIS location, but is also affected by the antenna array size and orientation of AP and UE. In addition, when the AP has a larger amount of antennas than UE, it is advantageous to place the RIS near the UE rather than the AP to achieve better channel condition. Modulation and coding schemes are applied in the simulations for comparison and capacity improvement is witnessed. Beneficial suggestions for RIS deployment in the MIMO system are concluded according to the simulation results.

INDEX TERMS MIMO communications, reconfigurable intelligent surface, rank analysis, capacity improvement.

I. INTRODUCTION

Reconfigurable intelligent surface (RIS), also known as intelligent reflecting surface (IRS) [1], large intelligent surface (LIS) [2], among others [3], [4], has become a hot topic in wireless communication community as it brings in new opportunity for fading and blockage settlement in high frequency for beyond-5G and future 6G communications. RIS consists of a large number of specially designed elements in the size of sub-wavelength [5], [6]. These elements form a low-profile 2D reflecting or transmission array, which is able to manipulate the phase, amplitude, polarization or frequency of the incident electromagnetic waves. With the tunable electronic circuit embedded in the element, for example [7], [8], a reflection-type RIS is able to steer the incident wave of a specific frequency band to the desired reflecting direction in real time, generating an anomalous reflection [9] rather than a specular reflection, and thus is capable of creating an intelligent electromagnetic environment for wireless communications [10], [11].

When it comes to high frequency regime, path loss and signal blockage become severe in wireless communications, which seriously limits the service range of an access point (AP) and lowers the transmission energy efficiency. RIS is found to be a low-cost and promising technique for combating blockage and path loss [12], [13] and outperforms its counterpart relay nodes [14]–[16]. Integrating the RIS into current MIMO system is one of the prevalent research recently. Achievable rate in the RIS-aided SISO system was analyzed in [17] and the author found that the codelength can be greatly reduced when RIS was employed in the system. RIS was applied for optimizing the channel capacity in [18]

The associate editor coordinating the review of this manuscript and approving it for publication was Cunhua Pan.

for indoor millimeter-wave (mmWave) MIMO communications and two optimization schemes were provided. Passive beamforming and receiver design for enhancing the uplink transmission were proposed in [19] for the RIS-aided multi-user MIMO system whereas the balance between power efficiency and spectral efficiency was discussed in [20]. Cutoff rate was adopted in [21] as the metric for mutual information optimization in RIS-aided MIMO system optimization. Efforts have been put into signal enhancement, service range extension [22], [23] and relevant researches for RIS applications, such as beamforming design [1], [24], energy efficiency optimization [25] and channel estimation [26], [27].

The direct link between the AP and UE is usually set to be blocked or the signal of the line-of-sight (LOS) path is assumed to be extremely weak and can be neglected in many of the recent studies, so as to highlight the ability of RIS for tackling the blockage and path loss in high frequency communications. Nevertheless, do we need RIS when there is no blockage and the receiving signal strength is good in wireless communications? Considering the MIMO system in a central park or a golf course covered by grass land and bushes but with rare buildings nearby, the lack of multi-path reflectors in the environment leads to a rank-deficient channel. Hence, the channel capacity is limited even if the UE has two or more receiving antennas. In a spacious public square where only the LOS signal is significant, the MIMO channel is also rank-deficient. Based on these rank-deficient scenes, this paper investigates the rank and capacity improvement by introducing RIS to the MIMO system.

Rank improvement in single-user MIMO system was reported in [28], but the antenna array sizes and orientations of both AP and UE are fixed in their study. We implement a simulation platform for RIS-assisted MIMO system, in which flexible location, orientation and array size are allowed for AP, UE and RIS. The array size refers to the number of antennas of the 2D antenna array equipped at AP or UE and the number of reflecting or transmission element of the 2D array mounted on a RIS board. The commonly used uniform rectangle array (URA) configuration is chosen in our simulations and the array size is denoted as number of rows times number of columns. A new model is chosen for evaluating the path loss of the cascaded RIS-scattering channels. The reciprocal condition number of the channel are calculated for different distances between AP and UE for rank analysis. The location of RIS is also taken into consideration and the distributions of reciprocal condition number are obtained with in a squared region. The impacts of array size of AP and the relative orientation between AP and UE to the rank improvement are also analyzed. In addition, modulation and coding schemes (MCS) [29] are considered in the capacity calculation. Uniform power allocation, instead of water-filling algorithm as in [28], is adopted in the simulations. Optimal installing location and orientation for RIS in MIMO system was discussed in [30] according to the signal-noise-ratio (SNR) at UE, but only the non-line-of-sight (NLOS) path is of concern. The optimization of RIS orientation and location for coverage extension was presented in [31] but a full picture of the capacity distribution within the coverage area was not given. This paper, on the other hand, inspects the performance improvement of MIMO system with the assistance of RIS when both LOS and RIS-scattering paths exist between the AP and UE. Our simulations and analysis offer insight into the characteristics of RIS-assisted MIMO channel, which helps clarify some important issues for RIS deployment.

The rest of the paper is organized as follows. Section II introduces the channel model of the RIS-assisted MIMO system under the local coordinates and far-field assumption. Section III presents simulation data and analysis of the RIS-assisted MIMO system. The impacts of AP-to-UE distance, array size and orientation of AP to the condition of the channel are investigated. The optimal location for RIS placement is also discussed in the simulations. Channel capacity of the LOS channel and that of the RIS-assisted channel are then compared. Besides the Shannon capacity, capacity of 64QAM and 256QAM schemes are also calculated for comparison. The capacity distributions under 256QAM scheme within the service area of a RIS are simulated under two scenarios: (1) UE with fixed orientation, (2) UE with random orientation. Finally, the conclusion is drawn according to the simulation results.

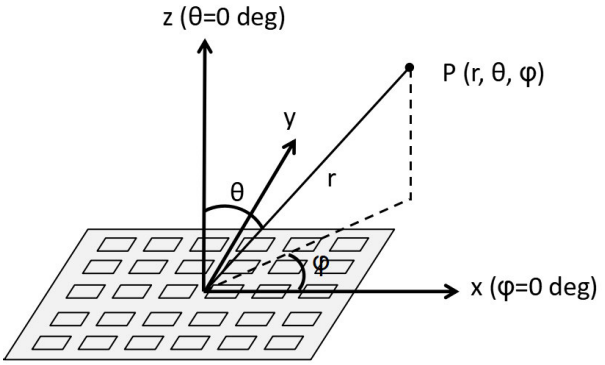

FIGURE 1. Local coordinates for a given array.

II. SYSTEM MODEL

As shown in Fig. 1, we first introduce a local spherical coordinates and a local Cartesian coordinates for a given antenna array. The origin of both coordinates locates at the center of the array and the pole axis of the spherical coordinates coincides with the positive z-axis of the Cartesian coordinates. It is more convenient to analyze the channel characteristics with the elevation angle θ and azimuth φ in the local spherical coordinates, where $\theta \in [0, \pi]$ and $\varphi \in [0, 2\pi]$. The spherical coordinate is also used as a global coordinates for depicting the location and orientation of the antenna arrays in this paper. The location and orientation of an array can be determined by the array center (x_c, y_c, z_c), the elevation angle θ and the azimuth φ, where θ is the angle spanned

by the positive z-axis and the normal vector of the array and φ is the angle spanned by the positive x-axis and the projection of the normal vector of the array on the x-y plane. For example, if the array lies in x-z plane with normal vector $\mathbf{n} = (0, -1, 0)$, then $\theta = \pi/2$ and $\varphi = 3\pi/2$.

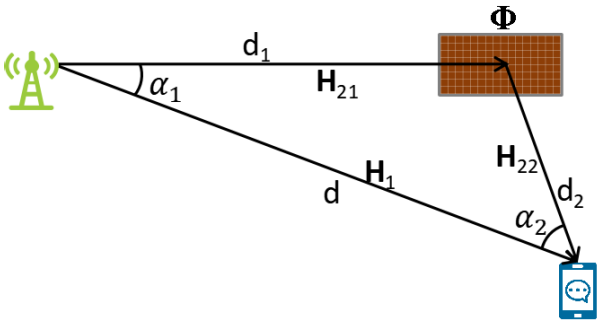

FIGURE 2. RIS-assisted wireless communication system model.

TABLE 1. AoD and AoA pairs in AP-RIS-UE system.

Source	Destination	Channel	AoD	AoA
AP	UE	$\mathbf{H}_1$	$(\theta_{12}, \varphi_{12})$	$(\theta_{21}, \varphi_{21})$
AP	RIS	$\mathbf{H}_{21}$	$(\theta_{13}, \varphi_{13})$	$(\theta_{31}, \varphi_{31})$
RIS	UE	$\mathbf{H}_{22}$	$(\theta_{32}, \varphi_{32})$	$(\theta_{23}, \varphi_{23})$

The RIS-assisted MIMO system considered in this paper consists of an AP with $N_t = N_{t,x} \times N_{t,y}$ antennas, a UE with $N_r = N_{r,x} \times N_{r,y}$ antennas and a RIS with $M = M_x \times M_y$ elements, as shown in Fig 2. The subscript x and y indicate the direction of the given array as shown in Fig. 1. Only reflection-type RIS is considered in this paper. We denote the antenna spacing of AP and UE as d_t and d_r respectively and the spacing of reflecting element of RIS as d_R. The signal received at UE can be expressed as

$$\mathbf{y} = \left(\sqrt{\beta_1}\mathbf{H}_1 + \sqrt{\beta_2}\mathbf{H}_{22}\Phi\mathbf{H}_{21}\right)\mathbf{w}\mathbf{s} + \mathbf{n}, \tag{1}$$

where $\mathbf{H}_1 \in \mathbb{C}^{N_r \times N_t}$ is the LOS channel between the AP and the UE whereas $\mathbf{H}_{21} \in \mathbb{C}^{M \times N_t}$ and $\mathbf{H}_{22} \in \mathbb{C}^{N_r \times M}$ are the cascaded channels between AP and RIS and between RIS and UE, respectively. Both $\mathbf{H}_{21}$ and $\mathbf{H}_{22}$ are assumed to be LOS channels due to the lack of surrounding reflectors. The gains of the AP-to-UE path and RIS-scattering path are denoted as β_1 and β_2, respectively. The diagonal matrix $\Phi \in \mathbb{C}^{M \times M}$ represents the phase shift imposed to the incident wave by the RIS elements and $\mathbf{w} \in \mathbb{C}^{N_t \times K}$ is the beamforming precoder at AP for the K-stream information vector $\mathbf{s}$ to be transmitted to UE. The noise term $\mathbf{n}$ is assumed to be an additive white Gaussian noise vector with each entry of zero-mean and variance σ^2, i.e. $\mathbf{n} \sim \mathcal{CN}\left(0, \sigma^2\mathbf{I}\right)$. Under the far-field assumption, $\mathbf{H}_1$, $\mathbf{H}_{21}$ and $\mathbf{H}_{22}$ can be determined by the corresponding angle of departure (AoD) and angle of arrival (AoA) pairs listed in Table 1. The elevation angle θ and azimuth φ are defined in the local spherical coordinates (Fig. 1). Four steering vectors are obtained according to the AP-to-UE AoD and AoA,

$$\mathbf{V}_{12,x} = \left[1, e^{j\phi_{12,x}}, \cdots, e^{j(N_{t,x}-1)\phi_{12,x}}\right], \tag{2}$$

$$\mathbf{V}_{12,y} = \left[1, e^{j\phi_{12,y}}, \cdots, e^{j(N_{t,y}-1)\phi_{12,y}}\right], \tag{3}$$

$$\mathbf{V}_{21,x} = \left[1, e^{j\phi_{21,x}}, \cdots, e^{j(N_{t,x}-1)\phi_{21,x}}\right], \tag{4}$$

$$\mathbf{V}_{21,y} = \left[1, e^{j\phi_{21,y}}, \cdots, e^{j(N_{t,y}-1)\phi_{21,y}}\right], \tag{5}$$

where the phase gradients are calculated as following,

$$\phi_{12,x} = kd_t \sin\theta_{12}\cos\varphi_{12}, \tag{6}$$

$$\phi_{12,y} = kd_t \sin\theta_{12}\sin\varphi_{12}, \tag{7}$$

$$\phi_{21,x} = kd_r \sin\theta_{21}\cos\varphi_{21}, \tag{8}$$

$$\phi_{21,y} = kd_r \sin\theta_{21}\sin\varphi_{21}, \tag{9}$$

with $k = 2\pi/\lambda$, λ being the wave length of the carrier wave. The LOS channel $\mathbf{H}_1$ can then be expressed as

$$\mathbf{H}_1 = \left(\mathbf{V}_{21,x} \otimes \mathbf{V}_{21,y}\right)^H \left(\mathbf{V}_{12,x} \otimes \mathbf{V}_{12,y}\right), \tag{10}$$

where the operator $\otimes$ denotes a Kronecker product and the superscript H represents a conjugate transpose. Similarly, $\mathbf{H}_{21}$ and $\mathbf{H}_{22}$ can be calculated using the AoD-AoA pairs $[(\theta_{13}, \varphi_{13}), (\theta_{31}, \varphi_{31})]$ and $[(\theta_{32}, \varphi_{32}), (\theta_{23}, \varphi_{23})]$, respectively. With the design of the diagonal phase-shift matrix Φ at RIS, we can simplify the RIS-scattering channel as $\mathbf{H}_2 = \mathbf{H}_{22}\Phi\mathbf{H}_{21}$ and the overall channel of the communication system can be written as

$$\mathbf{H} = \sqrt{\beta_1}\mathbf{H}_1 + \sqrt{\beta_2}\mathbf{H}_2. \tag{11}$$

For the RIS-scattering path, different path loss models have been proposed [32]–[36] and we adopt the model in [36] which takes into account the incident and reflection angles of the electromagnetic wave on a RIS,

$$\beta_2 = g_t g_r \left(\frac{M_x M_z d_R^2}{4\pi d_1 d_2}\right)^2 \Gamma^2 \cos\theta_{31}\cos\theta_{32}, \tag{12}$$

where d_1, d_2 are the distances of the AP-to-RIS and RIS-to-UE paths and g_t, g_r are the transmitting and receiving gains. The following free-space path loss model is applied for the LOS channel between the AP and UE,

$$PL = 32.4 + 20\log_{10} f + 20\log_{10} d \text{ (dB)}, \tag{13}$$

where f and d denote the carrier frequency in GHz and the distance of the LOS path in meter. The gain of the AP-to-UE path can then be determined as $\beta_1 = g_t g_r 10^{(-PL/10)}$.

In far-field regime, we know that $\mathbf{H}_1$ is a rank-one matrix and no more than one stream can be transmitted to UE simultaneously regardless of UE with multiple antennas. The placement of a RIS as a passive beamforming component in the communication system gives rise to a new scattering path. The singular value decomposition (SVD) of the overall channel $\mathbf{H}$ offers a clear view of the rank improvement. The rank of the overall channel can be determined by the number of singular values that exceed a certain threshold. In practice,

the rank of the channel is the average value of repeated measurements and may be a non-integer value. For the UE with 1×2 antenna array, a condition number is defined as λ_1/λ_2, where λ_1 and λ_2 are the first and second singular values. A large condition number indicates a singular (or rank-deficient) channel. The condition number tends to be an unbounded value when λ_2 is extremely small and it is troublesome to generate smooth plot when such value is included in a data set. Hence, we prefer the reciprocal condition number (rcond),

$$\text{rcond} = \lambda_2/\lambda_1, \tag{14}$$

as the metric in this paper. The rcond is close to 1 if the overall channel $\mathbf{H}$ is well-conditioned whereas the rcond approaches zero if the channel is rank-deficient. The spectral efficiency, an indicator for the capacity of the system, can be calculated by the singular values as follow,

$$C = \sum_{k=1}^{N_r} \log_2 \left(1 + \frac{P_k \lambda_k^2}{\sigma^2}\right), \tag{15}$$

where P_k is the power allocated to the k-th stream signal and λ_k^2 is the k-th singular value of $\mathbf{H}\mathbf{H}^H$. Usually, the water-filling algorithm is applied for the power allocation to achieve the best spectral efficiency in MIMO system. However, when MCS is considered, 64QAM or 256QAM for example, there are occasions that the AP-to-UE path has excellent SNR (SNR saturation) whereas the SNR of RIS-scattering path is poor and the RIS-scattering path should be allocated more power, which is conflict with the water-filling strategy and other suitable algorithm should be considered. To balance the performance and complexity, the averaged power allocation method is preferred in industrial implementation.

Owing to the assumption that $\mathbf{H}_1$, $\mathbf{H}_{21}$ and $\mathbf{H}_{22}$ are LOS channels, by applying SVD to $\mathbf{H}_{21}$, $\mathbf{H}_{22}$,

$$\mathbf{H}_{21} = \mathbf{U}_1 \Sigma_1 \mathbf{V}_1^H, \tag{16}$$

$$\mathbf{H}_{22} = \mathbf{U}_2 \Sigma_2 \mathbf{V}_2^H, \tag{17}$$

the optimal phase-shift matrix Φ can be determined by the left-hand-side singular matrix $\mathbf{U}_1$ of $\mathbf{H}_{21}$ and the right-hand-side singular matrix $\mathbf{V}_2^H$ of $\mathbf{H}_{22}$. Similarly, the optimal precoder $\mathbf{w}$ for AP antenna array can be determined by the right-hand side singular matrix of the SVD result of the overall channel $\mathbf{H}$. Hence, the phase-shift matrix Φ at RIS and the precoder $\mathbf{w}$ at AP will not be involved in the channel analysis.

III. SIMULATION RESULTS

A. RECIPROCAL CONDITION NUMBER VERSUS AP-TO-UE DISTANCE

This section investigates the rcond of the RIS-assisted MIMO channel with different AP-to-UE distances. If the rcond is used as the metric of the MIMO channel, it is difficult to foretell the optimal location for the RIS placement when the AP and UE are fixed. For one thing, it is better to increase the angles spanned by the LOS path and the RIS-scattering path (α_1 and α_2 in Fig. 2), so as to weaken the correlation between the LOS channel $\mathbf{H}_1$and the RIS-scattering channel $\mathbf{H}_2$. In other words, the RIS should be placed far away from both the AP and UE. For another, the path loss of the RIS-scattering channel should be limited for good SNR, which means it is better to place the RIS close to the AP or UE. The optimal location for RIS placement should balance the path loss and channel correlation.

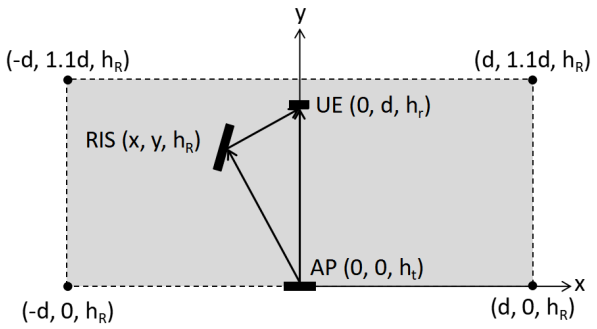

FIGURE 3. Top view of AP, UE locations and the squared region for RIS placement.

TABLE 2. Parameters for the simulation III-A.

Parameter	Value
Carrier frequency	f=3.5GHz
Array size of AP, UE and RIS (rows×columns)	$N_t = N_r = 1 \times 2, M = 16 \times 32$
Element spacing of AP, UE and RIS arrays	$d_t = d_r = d_R = 0.5\lambda$
Heights of AP, UE and RIS	$h_t = 12\text{m}, h_r = 1.5\text{m}, h_R = 3.5\text{m}$
Horizontal distance between AP and UE	$d = 30\text{m}, 90\text{m}, 200\text{m}$
Orientations of AP	$\theta_t = \pi/2, \varphi_t = \pi/2$
Orientations of UE	$\theta_r = \pi/2, \varphi_r = 3\pi/2$
Transmitting power per element	$P_t = 5\text{dBm}$
Noise power	$\sigma^2 = -97\text{dBm}$
Antenna gains at AP and UE	$G_t = G_r = 3\text{dBi}$
Reflection coefficient of RIS elements	Γ=0.8

In order to find out the impact of the RIS location to the rcond value, a squared region bounded by the AP and UE locations (Fig. 3) is traversed with fixed sampling spacing $\Delta d = 1\text{m}$ in x- and y-direction and each sampling site is a candidate for placing a RIS. The simulation is carried out with the parameters summarized in Table 2. For each sampling site in the squared region, optimal orientation and phase-shift matrix Φ is assumed for the RIS. The orientation that minimizes the incident and reflected angle θ_{31} and θ_{32} is chosen as the optimum [9], [36], which enhances the beamforming gain of the RIS-scattering beam thereby. The overall channel $\mathbf{H}$ then can be calculated by (1)-(13) for each RIS location and the rcond value corresponding to the RIS location can be obtained by (14).

The simulation results are shown as contour plots (Fig. 4) with the value of each point in the contours represents the

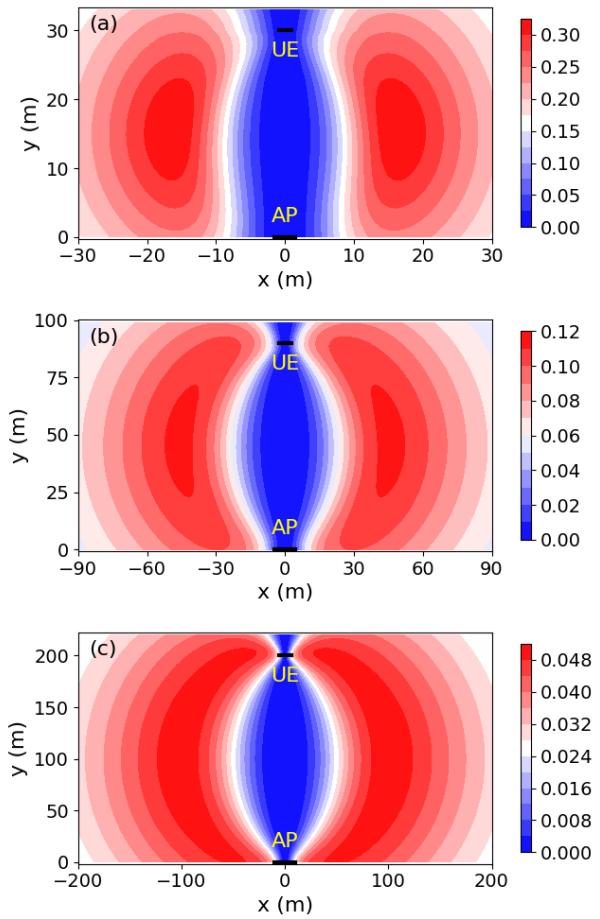

FIGURE 4. Contours of reciprocal condition number with horizontal distance between AP and UE d = 30m (a), 90m (b) and 200m (c). The solid black lines indicate the locations and orientations of AP and UE, but not represent the actual size of the antenna arrays.

reciprocal condition number of the overall channel of the RIS-assisted MIMO system when the RIS is placed at that position (with z = 3.5m). It is clear that there are extremely low value zones in the vicinity of the AP-to-UE LOS path for different AP-to-UE distance. Within these zones, the rcond value is close to zero and the channel rank is deficient. It is vainly to place a RIS in such zones for channel rank improvement. When the AP-to-UE distance increase, the total distance of the cascaded AP-to-RIS and RIS-to-UE paths is increased correspondingly and that leads to larger path loss. The path loss of the cascaded AP-RIS-UE path is more sensitive to the distance and the gain of the RIS-scattering path drops more than the AP-to-UE path. As a result, the rcond values become smaller with the increase of the AP-to-UE distance, but the rcond distributions keep symmetric. For the case d = 30m, the optimal location for RIS is (±15, 16, 3.5) and the maximum rcond value reaches 0.32 but for d = 200m, the maximum rcond value shrinks to 0.05 with RIS placed at (±101, 103, 3.5). Consequently, the RIS-assisted MIMO system will still be rank-deficient when the UE is extremely far away from the AP even when the RIS is not in the rank-deficient zone and the maximum AP-to-UE distance that a RIS is still applicable for rank improvement is yet to be determined by field test. The largest rcond value does not appear at the left or right boundary of the squared region, which proves that the optimal location for RIS is the place where the correlation and path loss between LOS channel and RIS-scattering channel are balanced.

A near-field model should be more accurate when the RIS is placed close to the AP or UE, but the simulation results are not affected significantly when the sampling sites are not extremely close to the AP or UE. In most scenarios, APs and UEs are usually not in the near-field region of the RIS, unless the RIS is used as a transmitting array [37], [38]. In addition, the beamforming gain of a near-field model is not guaranteed if accurate position information is not available and the performance of the system may not be as good as that with a far-field model.

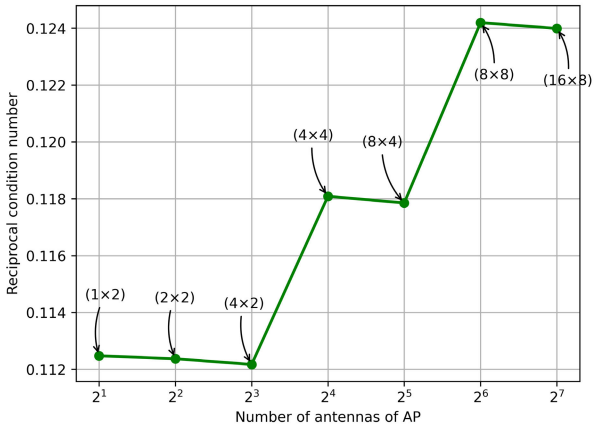

FIGURE 5. Reciprocal condition number versus array size of AP. The array shapes (rows × columns) are annotated at each data point.

B. RECIPROCAL CONDITION NUMBER VERSUS ANTENNA ARRAY SIZE AND ORIENTATION OF AP

According to (12), RIS with more reflecting elements, thereby larger array aperture, is more capable of coping with the path loss, which is coincident with the conclusion in previous researches [1], [24]. Under the same AP and UE configuration, greater rcond value of the overall channel can be obtained with RIS of more reflecting elements affirmatively. However, the impact of the antenna array size of AP on the rcond has not yet been discussed. In order to find out the potential impact of different antenna array size at AP side, we reuse the case d = 90 m in Section III-A and the parameters are identical to Table 2 except that the antenna array size of AP N_t is chosen to be 1 × 2, 2 × 2, 4 × 2, 4 × 4, 8 × 4, 8 × 8 and 16 × 8. Besides, the RIS is fixed at (−46, 47, 3.5), where the maximum rcond value is obtained (Fig. 4b). For this RIS location, the optimal orientation for RIS is $\theta = 86.04°$ and $\varphi = 1.05°$. Accordingly, we have $\theta_{31} = 45.09°$, $\varphi_{31} = 173.29°$, $\theta_{32} = 45.09°$, $\varphi_{32} = 353.29°$ and the simulation results are shown in Fig. 5. An interesting 3-step rcond curve with slight drops in each step section is

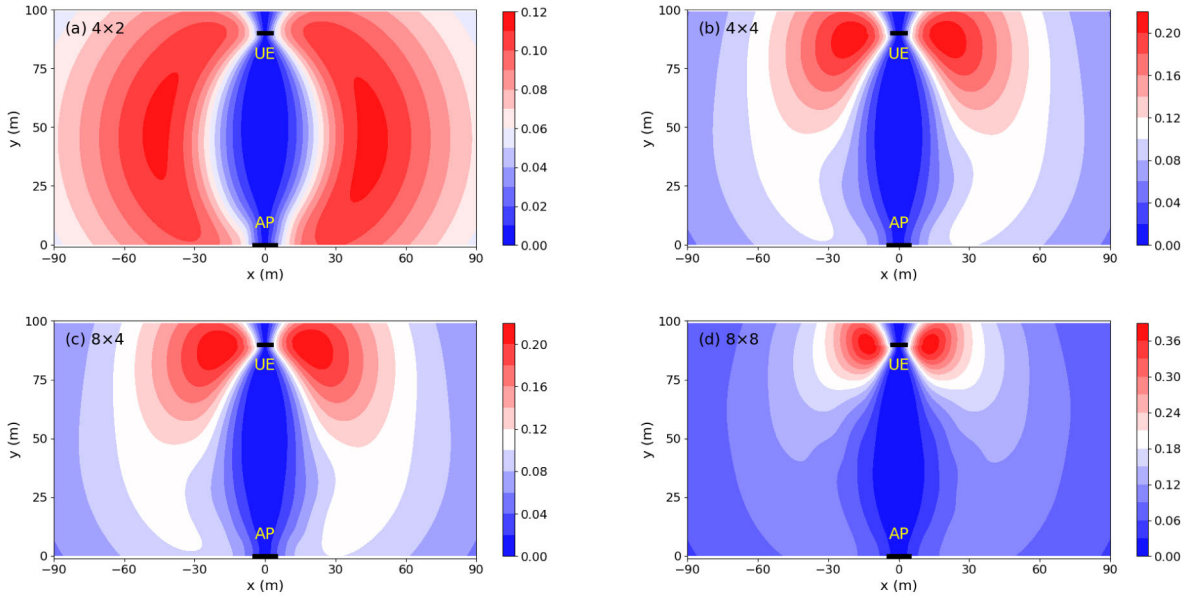

FIGURE 6. Contours of reciprocal condition number with AP of array sizes (a) 4 × 2, (b) 4 × 4, (c) 8 × 4 and (d) 8 × 8.

witnessed along with the increase of the number of antennas, which is quite counter-intuitive but also reasonable. One inconspicuous clue is that the array size of AP only increases in vertical direction at each step section of the rcond curve. For instance, the first step section has 3 data points and each point is obtained under the same number of antennas in horizontal direction and increasing number of antennas in vertical direction.

From the beamforming point of view, the increase of number of antennas in vertical direction narrows the transmitting beam in vertical direction and thus enhances the vertical resolution of the channel. In other words, the correlation between $\mathbf{H}_1$ and $\mathbf{H}_2$ in vertical direction will be weakened. However, the locations of AP, UE and RIS indicate that the correlation between channel $\mathbf{H}_1$ and $\mathbf{H}_2$ relies more on the resolution of the transmitting beam in horizontal direction. Furthermore, the horizontally aligned 1×2 antenna array at UE side is in lack of vertical resolution and thus is not sensitive to the beam width in vertical direction. As a result, the increase of antenna array size at AP side in vertical direction does not mitigate the correlation between $\mathbf{H}_1$ and $\mathbf{H}_2$ significantly and three steps appear in the rcond curve in Fig. 5. The slight drop in each step section in rcond value, on the other hand, is due to the different beamforming gain of the AP antenna array at different transmitting direction. A beam transmitted at normal direction of a given antenna array has larger beamforming gain than those transmitted in oblique direction and the beamforming gain is roughly proportional to the square of the array size, which indicates that the difference of the beamforming gain between normal-direction and oblique-direction transmission will be enlarged when the array size increases. Consequently, when the array size only increase in vertical direction, the correlation between the LOS channel and the RIS-scattering channel is almost unchanged, but the power gain difference between the two channels are amplified, and the superposition of these two factors leads to a slight drop in each step section of the rcond curve in Fig. 5. It should be noted that the rcond value is merely increased by 10.2% when the number of AP antennas changes from 2 to 128 for this RIS location.

To further address the impact of the antenna array size of AP to the RIS-assisted MIMO system, we traverse the squared region again for the rcond distributions corresponding to different AP configurations and the rcond values are contoured in Fig. 6. The rcond distribution changes scarcely when the antenna array size increase only in vertical direction (Fig. 6b and c), which is similar to the conclusion of Fig. 5. However, with the increase of the AP array size in horizontal direction, the maximum rcond value increases significantly and the optimal location for the RIS placement moves towards UE side. Consequently, the optimal location for RIS placement is also affected by the array sizes of AP and UE. Slight asymmetry with respect to the LOS path between AP and UE are shown in the rcond contours in Fig. 6 and the Kronecker-product-type channel model should account for such asymmetry.

The antenna arrays of AP and UE are assumed to be in perfect alignment in previous simulations. However, due to its mobility, the UE is not always in good alignment with AP in real environment. Based on the previous simulation setup (d = 90 m), we next probe into the situation that the AP and UE are not perfectly aligned. The antenna array size of AP is set to be 8×8 and three orientations of UE, $\varphi_r = 120°$, 150° and 180°, are chosen for comparison while other parameters are kept unchanged. The rcond contours for different UE orientations (Fig. 7) clearly illustrate that when the AP and UE

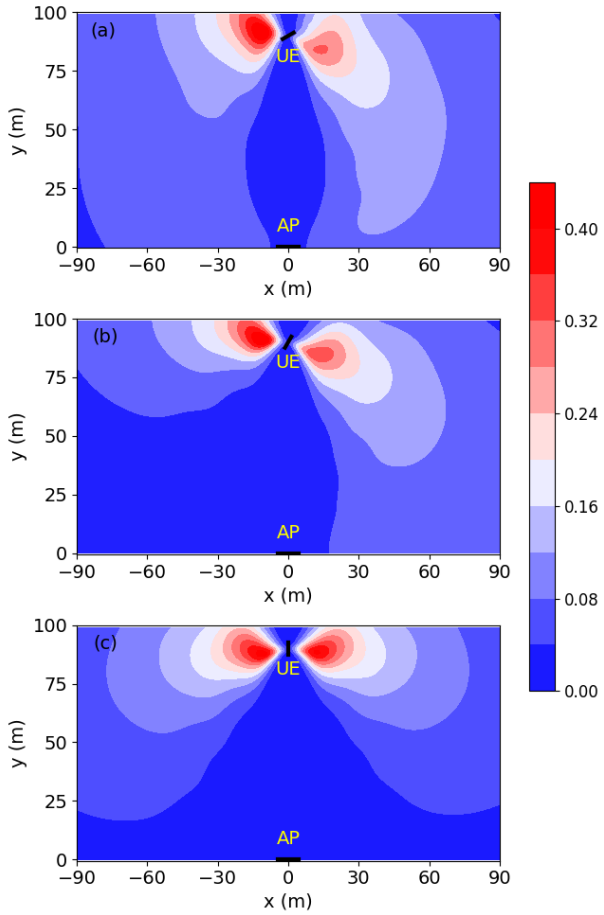

FIGURE 7. Contours of reciprocal condition number with different UE orientation; (a) $\varphi_r = 120°$, (b) $\varphi_r = 150°$, (c) $\varphi_r = 180°$.

antenna arrays are not perfectly aligned, the spatial pattern of rcond value rotates with UE but the maximum values are still lies in the vicinity of UE. Moreover, the rank-deficient zone is enlarged when $\varphi_r = 150°$ and 180°, compared with Fig. 6(d). That means the region which is suitable for RIS placement shrinks when the antenna arrays of AP and UE are not perfectly aligned. Moreover, these results imply that there is no absolute optimal location for RIS placement unless the UE orientation never changes. Fortunately, this problem is alleviated when another metric, channel capacity, rather than the rcond value is of concern, as demonstrated in the following section.

C. CAPACITY UNDER MODULATION AND CODING SCHEMES

The rcond value measures the rank of the RIS-assisted MIMO channel but does not indicate the channel capacity directly. To find out the capacity improvement with the assistance of RIS, the case of different antenna array sizes discussed in Section III-B (Fig. 5) is reconsidered. When MCS is considered in real communication system, 64QAM or 256QAM for example, the solution by water-filling algorithm may

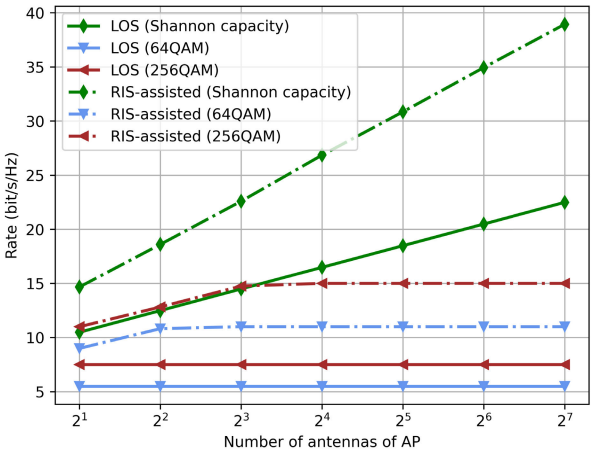

FIGURE 8. Comparison of channel capacity with and without the assistance of a RIS at a fixed location.

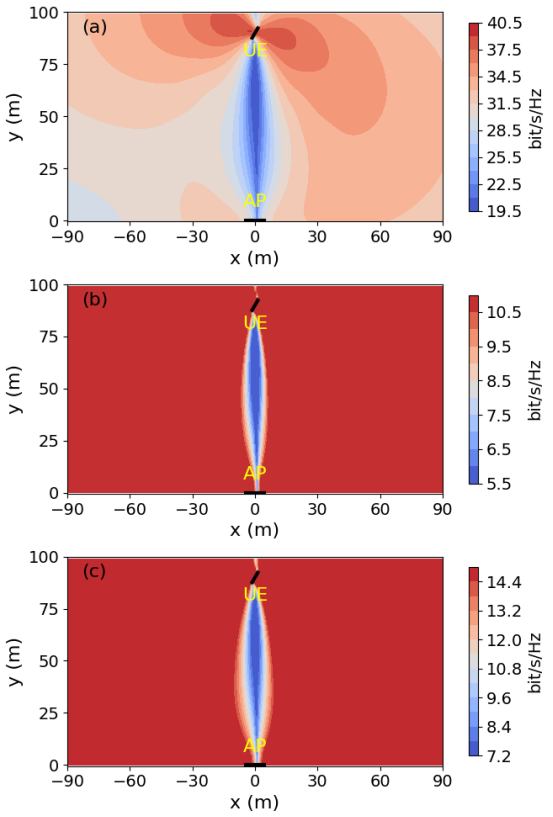

FIGURE 9. Contours of (a) Shannon capacity, (b) capacity under 64QAM scheme and (c) capacity under 256QAM scheme.

not be optimal anymore and uniform power allocation is preferred in wireless communication industry as a trade-off between performance and system complexity. As shown in Fig. 8, the Shannon capacity and capacities under 64QAM and 256QAM schemes are simulated with uniform power allocation strategy (dashed curves) and compared with the capacities in the absence of a RIS (solid curves). Obviously, the classical Shannon capacity increases steadily with the

number of AP antennas. Compared with the MIMO system with only LOS channel, the Shannon capacity of the RIS-assisted MIMO system is improved significantly. The channel capacity under 64QAM and 256QAM schemes are doubled compared with LOS channel capacity when enough antennas are equipped at the AP side but the capacity stops increasing when the number of AP antennas reaches a certain amount, which can be regarded as an SNR saturation. That is, when the SNR reaches a certain threshold, continuously increase of the SNR will not promote the channel capacity anymore.

When channel capacity is adopted as the metric for choosing the optimal RIS location, we would like to verify that whether the optimal location for RIS is the same as that indicated in the rcond contours in previous simulations. Reconsidering the case that d = 90m and $\varphi_r = 150°$ (Fig. 7b), the Shannon capacity and capacities with MCS are simulated for each sampling site in the squared region (Fig. 9). The Shannon capacity are higher when the RIS is close to UE (Fig. 9a), which is in agreement with the rcond distribution in Fig 7(b) and the low capacity region partially overlaps the rank-deficient zone as in Fig. 7(b). The large incident and reflection angles θ_{31} and θ_{32} at RIS account for this low capacity region as only feeble beamforming gain is obtained at UE from the RIS-scattering path as indicated by (12). For the 64QAM and 256QAM schemes, the capacity contours are less coupled with the rcond distributions and same capacity is achieved in most sampling sites (Fig. 9b and 9c). That means the optimal RIS location is no longer confined in a small region when MCS is applied, which is a good news for RIS deployment. Extremely low rcond value zones are found in Fig. 4, but it is hard to determine the exact range of rank-deficient zone. The capacity contour in which MCS is applied, on the other hand, shows a clear rank deficient zone in the squared region and an applicable threshold of singular value for determining the channel rank can be estimated.

The UE is assumed to be static in previous simulations to investigate the impact of RIS location to the channel capacity. In fact, UEs are usually moving targets while AP and RIS are fixed in most cases. It is important to investigate the capacity distribution within the service area of the RIS, so as to analyze whether there are rank-deficient zones in the service area. Hence, a simulation with fixed AP and RIS are carried out and capacities within a service area bounded by the AP and RIS are simulated without MCS scheme. The AP locates at (0, 50, 12) with $\theta_t = \pi/2$, $\varphi_t = 0$, $N_t = 8 \times 8$ and the RIS locates at (100, 0, 3.5) with $\theta_R = \pi/2$, $\varphi_R = \pi/2$, $M = 16 \times 32$. Two cases are designed for comparison. For case 1, the UE moves in the service area with fixed orientation $\varphi_r = 45°$. For case 2, the UE alters its orientation randomly within the service area. The simulation results show that there is a narrow low-capacity stripe in the LOS path between AP and RIS in both cases. Low capacity also appears in the vicinity of the lower boundary of the service area, which is resulted from the weak beamforming ability of RIS at these large reflection angle. The low capacity region near the right boundary of the service area, on the other hand, is due to the large path loss in this region. The capacity contour of the random-orientation case is similar to the corrosion effect in the image process, compared with fixed-orientation case, but the capacity distributions are roughly matched and the low-capacity stripe still exists in the random-orientation case. The good news is that capacity improvement is witnessed near the right boundary in random-orientation case. Hence, the alteration of UE in real applications will not degrade the system performance. Besides, users usually change the orientation of their equipment smoothly in daily life and no abrupt drop of the transmission rate is to occur within the service area.

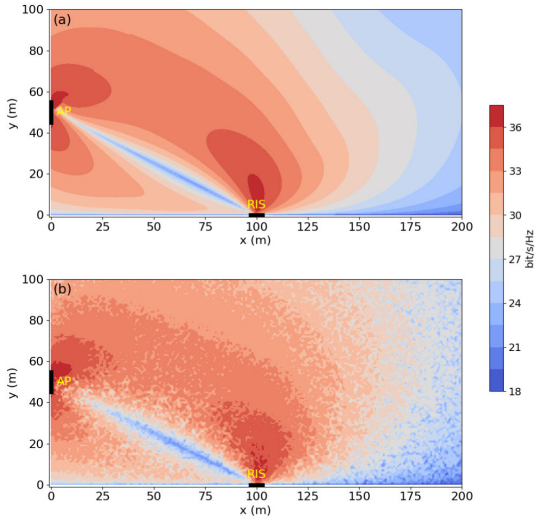

FIGURE 10. Contours of channel capacity with (a) fixed and (b) random UE orientation within the RIS service area.

With the above simulations and analysis, some beneficial insights for the RIS-assisted MIMO system are obtained and important issues concerning RIS deployment can be outlined. For one thing, the placement of a RIS at a proper location do help improve the rank and capacity of the MIMO system but the optimal location for RIS varies with the orientation of UE according to the rcond value. It is better to place the RIS near the UE for capacity improvement when the antenna array size of AP is larger than that of UE. For another, there is still rank-deficient zone despite of the deployment of a RIS. The rank-deficient zone lies in the vicinity of the LOS path between AP and UE in the case that AP and UE are fixed and RIS installment in such zone should be avoided. The rank-deficient zone lies in the LOS path between AP and RIS in the case that AP and RIS are fixed and no capacity improvement is expected when UE moves in such zone. Additionally, the application of MCS (64QAM and 256QAM for example) lowers the capacity improvement but the optimal location for a RIS is easier to be determined as the rank-deficient zone is confined to a narrower region. As it is mentioned in Section I, when it comes to mmWave band or even terahertz band, the path loss becomes severe and the service range of a RIS will be shrank. However, the channel becomes

sparse [39], [40] and the rank of the channel tends to be deficient in higher frequency, especially in terahertz band. Hence, RIS is going to play a more important role in mmWave band and terahertz band.

IV. CONCLUSION

The rank and capacity improvement of the MIMO system with the assistance of a RIS is discussed in this paper. With various simulations, the spatial characteristics of the RIS-assisted MIMO system is investigated. The impact of RIS location, antenna array size of AP and relative orientation between AP and UE to the system are taken into consideration in the simulations. The capacity improvements under MCS are also simulated and compared with the classical Shannon capacity. Rank-deficient zones are found in the RIS-assisted MIMO system which offers guide for RIS deployment and coverage area planning. The antenna array size of AP plays a limited role in channel rank improvement when RIS location is fixed. When MCS is considered in real communication applications, the reciprocal condition number is no longer a good metric for the selection of optimal RIS location due to the SNR saturation effect. The changeful UE orientation adds to the complexity of finding an optimal location for RIS placement as the rank-deficient zone will be distorted and expanded in some occasion. The mobility and randomly orientation variation of UE also give rise to capacity fluctuation within the RIS service area, but fortunately, capacity improvement can still be expected within the service area.

REFERENCES

[1] Q. Wu and R. Zhang, "Intelligent reflecting surface enhanced wireless network: Joint active and passive beamforming design," in *Proc. IEEE Global Commun. Conf. (GLOBECOM)*, Dec. 2018, pp. 1–6, doi: 10.1109/GLOCOM.2018.8647620.

[2] S. Hu, F. Rusek, and O. Edfors, "Beyond massive MIMO: The potential of data transmission with large intelligent surfaces," *IEEE Trans. Signal Process.*, vol. 66, no. 10, pp. 2746–2758, May 2018, doi: 10.1109/TSP.2018.2816577.

[3] C. Liaskos, S. Nie, A. Tsioliaridou, A. Pitsillides, S. Ioannidis, and I. Akyildiz, "A new wireless communication paradigm through software-controlled metasurfaces," *IEEE Commun. Mag.*, vol. 56, no. 9, pp. 162–169, Sep. 2018.

[4] X. Tan, Z. Sun, D. Koutsonikolas, and J. M. Jornet, "Enabling indoor mobile millimeter-wave networks based on smart reflect-arrays," in *Proc. IEEE Conf. Comput. Commun. (INFOCOM)*, Apr. 2018, pp. 270–278, doi: 10.1109/INFOCOM.2018.8485924.

[5] S. V. Hum and J. Perruisseau-Carrier, "Reconfigurable reflectarrays and array lenses for dynamic antenna beam control: A review," *IEEE Trans. Antennas Propag.*, vol. 62, no. 1, pp. 183–198, Jan. 2014, doi: 10.1109/TAP.2013.2287296.

[6] F. Yang and Y. Rahmat-Samii, *Surface Electromagnetics: With Applications in Antenna, Microwave, and Optical Engineering*. Cambridge, U.K.: Cambridge Univ. Press, Jun. 2019, pp. 30–37.

[7] L. Dai, B. Wang, M. Wang, X. Yang, J. Tan, S. Bi, S. Xu, F. Yang, Z. Chen, M. Di Renzo, C.-B. Chae, and L. Hanzo, "Reconfigurable intelligent surface-based wireless communications: Antenna design, prototyping, and experimental results," *IEEE Access*, vol. 8, pp. 45913–45923, 2020, doi: 10.1109/ACCESS.2020.2977772.

[8] W. Tang, M. Z. Chen, J. Y. Dai, Y. Zeng, X. Zhao, S. Jin, Q. Cheng, and T. J. Cui, "Wireless communications with programmable metasurface: New paradigms, opportunities, and challenges on transceiver design," *IEEE Wireless Commun.*, vol. 27, no. 2, pp. 180–187, Apr. 2020, doi: 10.1109/MWC.001.1900308.

[9] A. Díaz-Rubio, V. S. Asadchy, A. Elsakka, and S. A. Tretyakov, "From the generalized reflection law to the realization of perfect anomalous reflectors," *Sci. Adv.*, vol. 3, no. 8, Aug. 2017, Art. no. e1602714, doi: 10.1126/sciadv.1602714.

[10] M. Di Renzo, A. Zappone, M. Debbah, M.-S. Alouini, C. Yuen, J. de Rosny, and S. Tretyakov, "Smart radio environments empowered by reconfigurable intelligent surfaces: How it works, state of research, and the road ahead," *IEEE J. Sel. Areas Commun.*, vol. 38, no. 11, pp. 2450–2525, Nov. 2020, doi: 10.1109/JSAC.2020.3007211.

[11] Q. Wu and R. Zhang, "Towards smart and reconfigurable environment: Intelligent reflecting surface aided wireless network," *IEEE Commun. Mag.*, vol. 58, no. 1, pp. 106–112, Jan. 2020, doi: 10.1109/MCOM.001.1900107.

[12] M. A. Kishk and M.-S. Alouini, "Exploiting randomly located blockages for large-scale deployment of intelligent surfaces," *IEEE J. Sel. Areas Commun.*, vol. 39, no. 4, pp. 1043–1056, Apr. 2021, doi: 10.1109/JSAC.2020.3018808.

[13] G. Zhou, C. Pan, H. Ren, K. Wang, M. Elkashlan, and M. D. Renzo, "Stochastic learning-based robust beamforming design for RIS-aided millimeter-wave systems in the presence of random blockages," *IEEE Trans. Veh. Technol.*, vol. 70, no. 1, pp. 1057–1061, Jan. 2021, doi: 10.1109/TVT.2021.3049257.

[14] A.-A.-A. Boulogeorgos and A. Alexiou, "Performance analysis of reconfigurable intelligent surface-assisted wireless systems and comparison with relaying," *IEEE Access*, vol. 8, pp. 94463–94483, 2020, doi: 10.1109/ACCESS.2020.2995435.

[15] M. Di Renzo, K. Ntontin, J. Song, F. H. Danufane, X. Qian, F. Lazarakis, J. De Rosny, D.-T. Phan-Huy, O. Simeone, R. Zhang, M. Debbah, G. Lerosey, M. Fink, S. Tretyakov, and S. Shamai, "Reconfigurable intelligent surfaces vs. relaying: Differences, similarities, and performance comparison," *IEEE Open J. Commun. Soc.*, vol. 1, pp. 798–807, 2020, doi: 10.1109/OJCOMS.2020.3002955.

[16] E. Basar, M. Di Renzo, J. De Rosny, M. Debbah, M. Alouini, and R. Zhang, "Wireless communications through reconfigurable intelligent surfaces," *IEEE Access*, vol. 7, pp. 116753–116773, 2019, doi: 10.1109/ACCESS.2019.2935192.

[17] X. Liu, "On the achievable rate under finite codelength for RIS-aided systems," *IEEE Access*, vol. 9, pp. 116369–116375, 2021, doi: 10.1109/ACCESS.2021.3105287.

[18] N. S. Perovic, M. D. Renzo, and M. F. Flanagan, "Channel capacity optimization using reconfigurable intelligent surfaces in indoor mmWave environments," in *Proc. IEEE Int. Conf. Commun. (ICC)*, Jun. 2020, pp. 1–7, doi: 10.1109/ICC40277.2020.9148781.

[19] W. Yan, X. Yuan, Z.-Q. He, and X. Kuai, "Passive beamforming and information transfer design for reconfigurable intelligent surfaces aided multiuser MIMO systems," *IEEE J. Sel. Areas Commun.*, vol. 38, no. 8, pp. 1793–1808, Aug. 2020, doi: 10.1109/JSAC.2020.3000811.

[20] L. You, J. Xiong, D. W. K. Ng, C. Yuen, W. Wang, and X. Gao, "Energy efficiency and spectral efficiency tradeoff in RIS-aided multiuser MIMO uplink transmission," *IEEE Trans. Signal Process.*, vol. 69, pp. 1407–1421, 2021, doi: 10.1109/TSP.2020.3047474.

[21] N. S. Perović, L.-N. Tran, M. D. Renzo, and M. F. Flanagan, "Optimization of RIS-aided MIMO systems via the cutoff rate," *IEEE Wireless Commun. Lett.*, vol. 10, no. 8, pp. 1692–1696, Aug. 2021, doi: 10.1109/LWC.2021.3077579.

[22] M. Nemati, J. Park, and J. Choi, "RIS-assisted coverage enhancement in millimeter-wave cellular networks," *IEEE Access*, vol. 8, pp. 188171–188185, 2020, doi: 10.1109/ACCESS.2020.3031392.

[23] W. Khawaja, O. Ozdemir, Y. Yapici, F. Erden, and I. Guvenc, "Coverage enhancement for NLOS mmWave links using passive reflectors," *IEEE Open J. Commun. Soc.*, vol. 1, pp. 263–281, 2020, doi: 10.1109/OJCOMS.2020.2969751.

[24] Q. Wu and R. Zhang, "Beamforming optimization for intelligent reflecting surface with discrete phase shifts," in *Proc. IEEE Int. Conf. Acoust., Speech Signal Process. (ICASSP)*, May 2019, pp. 7830–7833, doi: 10.1109/ICASSP.2019.8683145.

[25] C. Huang, A. Zappone, G. C. Alexandropoulos, M. Debbah, and C. Yuen, "Reconfigurable intelligent surfaces for energy efficiency in wireless communication," *IEEE Trans. Wireless Commun.*, vol. 18, no. 8, pp. 4157–4170, Aug. 2019, doi: 10.1109/TWC.2019.2922609.

[26] H. Liu, X. Yuan, and Y.-J.-A. Zhang, "Matrix-calibration-based cascaded channel estimation for reconfigurable intelligent surface assisted multiuser MIMO," *IEEE J. Sel. Areas Commun.*, vol. 38, no. 11, pp. 2621–2636, Nov. 2020, doi: 10.1109/JSAC.2020.3007057.

[27] L. Wei, C. Huang, G. C. Alexandropoulos, C. Yuen, Z. Zhang, and M. Debbah, "Channel estimation for ris-empowered multi-user miso wireless communications," *IEEE Trans. Commun.*, vol. 69, no. 6, pp. 4144–4157, Jun. 2021, doi: 10.1109/TCOMM.2021.3063236.
[28] O. Özdogan, E. Björnson, and E. G. Larsson, "Using intelligent reflecting surfaces for rank improvement in MIMO communications," in *Proc. IEEE Int. Conf. Acoust., Speech Signal Process. (ICASSP)*, May 2020, pp. 9160–9164, doi: 10.1109/ICASSP40776.2020.9052904.
[29] *NR; Physical Layer Procedures for Data (Release 16)*, document TS 38.214, 3GPP, 2021. [Online]. Available: https://www.3gpp.org
[30] K. Ntontin, A.-A.-A. Boulogeorgos, D. G. Selimis, F. I. Lazarakis, A. Alexiou, and S. Chatzinotas, "Reconfigurable intelligent surface optimal placement in millimeter-wave networks," *IEEE Open J. Commun. Soc.*, vol. 2, pp. 704–718, 2021, doi: 10.1109/OJCOMS.2021.3068790.
[31] S. Zeng, H. Zhang, B. Di, Z. Han, and L. Song, "Reconfigurable intelligent surface (RIS) assisted wireless coverage extension: RIS orientation and location optimization," *IEEE Commun. Lett.*, vol. 25, no. 1, pp. 269–273, Jan. 2021, doi: 10.1109/LCOMM.2020.3025345.
[32] M. Di Renzo, F. H. Danufane, X. Xi, J. de Rosny, and S. Tretyakov, "Analytical modeling of the path-loss for reconfigurable intelligent surfaces—Anomalous mirror or scatterer?" in *Proc. IEEE 21st Int. Workshop Signal Process. Adv. Wireless Commun. (SPAWC)*, May 2020, pp. 1–5, doi: 10.1109/SPAWC48557.2020.9154326.
[33] W. Tang, M. Z. Chen, X. Chen, J. Y. Dai, Y. Han, M. Di Renzo, Y. Zeng, S. Jin, Q. Cheng, and T. J. Cui, "Wireless communications with reconfigurable intelligent surface: Path loss modeling and experimental measurement," *IEEE Trans. Wireless Commun.*, vol. 20, no. 1, pp. 421–439, Jan. 2021, doi: 10.1109/TWC.2020.3024887.
[34] O. Özdogan, E. Björnson, and E. G. Larsson, "Intelligent reflecting surfaces: Physics, propagation, and pathloss modeling," *IEEE Wireless Commun. Lett.*, vol. 9, no. 5, pp. 581–585, May 2020, doi: 10.1109/LWC.2019.2960779.
[35] F. H. Danufane, M. D. Renzo, J. de Rosny, and S. Tretyakov, "On the path-loss of reconfigurable intelligent surfaces: An approach based on Green's theorem applied to vector fields," *IEEE Trans. Commun.*, vol. 69, no. 8, pp. 5573–5592, Aug. 2021, doi: 10.1109/TCOMM.2021.3081452.
[36] W. Tang, X. Chen, M. Z. Chen, J. Y. Dai, Y. Han, M. Di Renzo, S. Jin, Q. Cheng, and T. J. Cui, "Path loss modeling and measurements for reconfigurable intelligent surfaces in the millimeter-wave frequency band," 2021, *arXiv:2101.08607*. [Online]. Available: http://arxiv.org/abs/2101.08607
[37] H. Kamoda, T. Iwasaki, J. Tsumochi, T. Kuki, and O. Hashimoto, "60-GHz electronically reconfigurable large reflectarray using single-bit phase shifters," *IEEE Trans. Antennas Propag.*, vol. 59, no. 7, pp. 2524–2531, Jul. 2011, doi: 10.1109/TAP.2011.2152338.
[38] H.-X. Xu, T. Cai, Y.-Q. Zhuang, Q. Peng, G.-M. Wang, and J.-G. Liang, "Dual-mode transmissive metasurface and its applications in multi-beam transmitarray," *IEEE Trans. Antennas Propag.*, vol. 65, no. 4, pp. 1797–1806, Apr. 2017, doi: 10.1109/TAP.2017.2673814.
[39] B. Peng, S. Rey, and T. Kürner, "Channel characteristics study for future indoor millimeter and submillimeter wireless communications," in *Proc. 10th Eur. Conf. Antennas Propag. (EuCAP)*, Apr. 2016, pp. 1–5, doi: 10.1109/EuCAP.2016.7481456.
[40] H. Zhang, R. He, B. Ai, S. Cui, and H. Zhang, "Measuring sparsity of wireless channels," *IEEE Trans. Cognit. Commun. Netw.*, vol. 7, no. 1, pp. 133–144, Mar. 2021, doi: 10.1109/TCCN.2020.3013270.

JUN YANG received the B.S. degree in geophysics from China University of Geosciences, Wuhan, in 2011, and the Joint-Training Ph.D. degree in geophysics from the University of Science and Technology of China and the University of North Carolina at Charlotte, in 2016. He is currently an Algorithm Engineer with ZTE Corporation. His research interests include reconfigurable intelligent surface, MIMO channel modeling, and computational electromagnetics.

YIJIAN CHEN received the B.S. degree from Central South University, in 2006. He is currently a Senior Engineer with ZTE Corporation. His current research interests include massive MIMO, coordinated multi-point transmission, high-frequency communications, and channel modeling.

MENGNAN JIAN received the B.E. degree in information engineering from Beijing Institute of Technology, Beijing, China, in 2016, and the M.S. degree from Tsinghua University, Beijing, in 2019. She is currently an Engineer with ZTE Corporation. Her research interests include orbital angular momentum and reconfigurable intelligent surface.

JIANWU DOU was born in Yuci, Shanxi, China, in 1973. He received the Ph.D. degree in robotic mechanism from Beijing University of Technology, Beijing, China, in July 2001. From 2000 to 2014, he was the Head of the Wireless RRM Team, including 2G/3G/4G/WLAN and was in charge of developing multi-RAT wireless system simulation platform. From 2005 to 2017, he was the Vice Director of the Wireless Algorithm Department, ZTE. From 2012 to 2014, he was the Product Manager of ZTE iNES, a multi-cell/multi-UE hardware wireless channel emulator. He was in charge of a National Major Project and participated in two 5G projects sponsored by the Ministry of Industry and Information Technology of China. His current research interests include 5G/B5G channel modeling, new air-interface, unmanned aerial vehicle, non-terrestrial network research, THz, meta-materials, and RIS. He received the Science and Technology Award (1st Level) in 2014 and 2015, and the Award for Chinese Outstanding Patented Invention in 2011, from China Institute of Communications and WIPO-SIPO, respectively.

MIN FANG received the Ph.D. degree from the Department of Electronic Engineering, Tsinghua University, in 1999. She joined ZTE Corporation, in 2004, and focused on the research, the standardization and the IPR for next generation wireless. She participated in all the standardization works of 3GPP LTE Release 8 by leading ZTE's FDD and EPC standard team. She also made an outstanding contribution to the ZTE's 5G Research and Development works on the Pre5G massive MIMO technology winning both the Best Mobile Technology Breakthrough and the CTO Choice awards in MWC 2016. She is currently the Director of 6G Research and Collaboration with the Wireless Division, ZTE. She is coordinating the wireless research activities on new services and spectrum, and the novel architecture and enablers towards 6G.